

Modeling seashells

Deborah R. Fowler^{†*}, Hans Meinhardt[‡] and Przemyslaw Prusinkiewicz[†]

[†]Department of Computer Science
University of Calgary
Alberta, Canada T2N 1N4

* Department of Computer Science
University of Regina
Canada

[‡]Max-Planck-Institut
für Entwicklungsbiologie
7400 Tübingen, Germany

From Proceedings of SIGGRAPH '92 (Chicago, Illinois, July 26–31, 1992),
In *Computer Graphics*, 26, 2, (July 1992), ACM SIGGRAPH, New York, pp. 379–387.

For technical reasons, the formatting of this paper
is slightly different from the original publication.

Modeling seashells

Deborah R. Fowler

Department of Computer Science
University of Calgary
and University of Regina
Canada

Hans Meinhardt

Max-Planck-Institut
für Entwicklungsbiologie
7400 Tübingen, Germany

Przemyslaw Prusinkiewicz

Department of Computer Science
University of Calgary
Alberta, Canada T2N 1N4

(Authors listed alphabetically)

ABSTRACT

This paper presents a method for modeling seashells, suitable for image synthesis purposes. It combines a geometric description of shell shapes with an activator-inhibitor model of pigmentation patterns on shell surfaces. The technique is illustrated using models of selected shells found in nature.

CR Categories: I.3.5 [Computer Graphics]: Computational Geometry and Object Modeling: *Curve, surface, solid and object representation.* I.3.7 [Computer Graphics]: Three-Dimensional Graphics and Realism. J.3 [Life and Medical Sciences]: *Biology.*

Keywords: realistic image synthesis, modeling of natural phenomena, seashell, logarithmic helico-spiral, sweep representation, reaction-diffusion pattern model.

1 INTRODUCTION

The beauty of shells invites us to construct their mathematical models. The motivation is to synthesize realistic images that could be incorporated into computer-generated scenes and to gain a better understanding of the mechanism of shell formation. The latter objective was crisply justified by Raup, the pioneer of computer modeling of shell morphology [28]:

Successful simulation provides confirmation of the underlying models as valid descriptions of the actual biological situation;

Unsuccessful simulation shows flaws in the postulated model and may suggest the changes that should be made in the model to correct the flaws;

Non-occurring forms, perhaps intermediate between actual species, may be simulated and thus may lead to a better understanding of the relationships between the real forms.

In this paper, we propose a modeling technique that combines two key components: a model of shell shapes derived from a descriptive

characterization by d'Arcy Thompson [31], and a reaction-diffusion model of pigmentation patterns originated by Meinhardt [17]. The results are evaluated by comparing models with the real shells.

Historically, the logarithmic spiral, capturing the essence of the shell shape, was first described in 1638 by Descartes [31, page 754] and applied to characterize shell coiling by Moseley [21]. By the beginning of the twentieth century, it was observed in many artificial and organic forms [4]. Moseley's characterization was supported experimentally and popularized by Thompson [31], who presented careful measurements of a wide variety of taxonomic and functional types of shells, and showed their conformity with the logarithmic model.

The application of computers to the visualization and analysis of shell shapes was originated by Raup. In the first paper devoted to this topic [27], he presented two-dimensional plots of longitudinal cross-sections of shells as a form of blueprints that may assist a person who is drawing shell forms. Subsequently, Raup extended his model to three dimensions [29], and visualized shell models as stereo pairs, using a wire-frame representation [28].

Kawaguchi [15] developed the first shell model intended specifically for computer graphics purposes. He enhanced the appearance of shell models using a polygon mesh instead of a wire frame. Similar representations were used subsequently by Oppenheimer [23], and Prusinkiewicz and Streibel [26]. Pursuing a different approach, Pickover [24, 25] approximated shell surfaces using interpenetrating spheres, placed at carefully chosen distances from each other and rendered using periodically altering colors to create the appearance of a ribbed surface with stripes.

The recent work on the modeling of shells has been characterized by an increased attention to detail. Illert [14] introduced Frenet frames [3, 7] to precisely orient the opening of the shell. His model also captured a form of surface sculpture. Cortie [5] allowed for independent tilting of the opening in three directions, presented models with the apertures defying simple mathematical description, and extended the range of surface ornateations captured by the model.

Our model of shell geometry is similar to that originated by Raup and culminating in the work of Cortie. It enhances previous models by applying free-form parametric curves (in the Bézier form) to capture the shape of shell aperture. However, the most conspicuous improvement results from the incorporation of pigmentation patterns into the models.

Mathematical modeling of pigmentation patterns was pioneered in 1969 by Waddington and Cowe [35], who reproduced patterns of *Oliva porphyria* using cellular automata. A similar formalism was

applied by Baker and Herman [1], and Wolfram [37]. According to Murray [22, page 506], these models had no basis in the underlying biological processes involved in the mollusc's growth. In 1984, Meinhardt introduced a biologically-motivated reaction-diffusion model [17], subsequently refined with Klinger [18, 19, 20]. Ermentrout, Campbell and Oster [8] proposed an alternative model employing neural nets. These two models share the basic mathematical concepts of short-range activation and long-range inhibition, and consequently yield similar patterns. We employ Meinhardt's model in our implementation.

From the computer graphics perspective, the use of reaction-diffusion processes [11, 16, 33] for image synthesis purposes was pioneered by Turk [34], and Witkin and Kass [36]. They focused on patterns defined by the distribution of morphogens in two-dimensional surfaces. In contrast, pigmentation patterns in shells are formed only along the growing edge of a shell. The second dimension results from the deposition of new shell material, which continually changes the position of the growing edge over time. Thus, the pattern on a shell can be viewed as a record of what has happened at the growing edge during the life span of a particular animal. This dynamic aspect sets the pigmentation patterns in shells apart from the reaction-diffusion models previously considered in computer graphics.

The organization of the paper follows the main division of the topic into the modeling of shell shapes (Section 2) and the generation of pigmentation patterns (Section 3). The results are evaluated in Section 4, which is concluded with a list of open problems.

2 MODELING SHELL GEOMETRY

In Chapter XI of *On Growth and Form* [31], d'Arcy Thompson provided a detailed description of shell geometry, supported by measurements of selected shells. Some of his observations are quoted below in a slightly edited form.

The surface of any shell may be generated by the revolution about a fixed axis of a closed curve, which, remaining always geometrically similar to itself, increases its dimensions continually. [...] Let us imagine some characteristic point within this closed curve, such as its centre of gravity. Starting from a fixed origin, this characteristic point describes an equiangular spiral in space about a fixed axis (namely the axis of the shell), with or without a simultaneous movement of translation along the axis. The scale of the figure increases in geometrical progression while the angle of rotation increases in arithmetical, and the centre of similitude remains fixed. [...] The form of the generating curve is seldom open to easy mathematical expressions.

Our modeling method is derived from this description.

2.1 The helico-spiral

The modeling of a shell surface starts with the construction of a logarithmic (equiangular) helico-spiral \mathcal{H} (Figure 1). In a cylindrical coordinate system (shown in Figure 1 as embedded in the Cartesian xyz system) it has the parametric description [6]:

$$\theta = t, \quad r = r_0 \xi_r^t, \quad z = z_0 \xi_z^t. \quad (1)$$

Parameter t ranges from 0 at the apex of the shell to t_{max} at the opening. The first two equations represent a logarithmic spiral lying

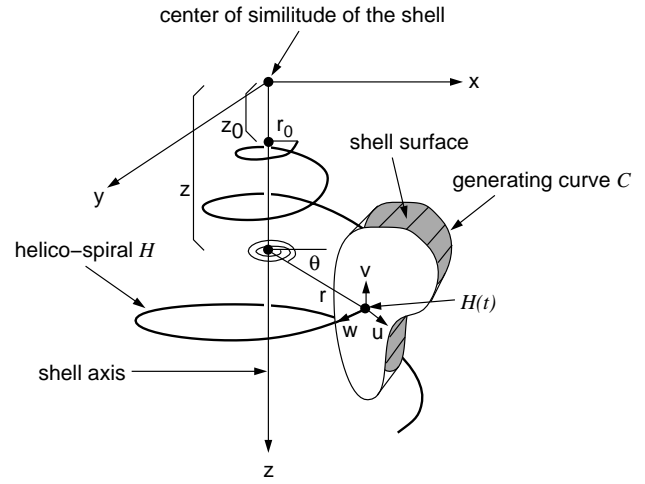


Figure 1: Construction of the shell surface

in the plane $z = 0$. The third equation stretches the spiral along the z -axis, thus contributing a helical component to its shape.

Distances r and z are exponential functions of the parameter t , and usually have the same base, $\xi_r = \xi_z = \xi$. As a result, the generating helico-spiral is self-similar, with the center of similitude located at the origin of the coordinate system xyz . Given the initial values θ_0 , r_0 , and z_0 , a sequence of points on the helico-spiral can be computed incrementally using the formulae:

$$\begin{aligned} \theta_{i+1} &= t_i + \Delta t &= \theta_i + \Delta\theta, \\ r_{i+1} &= r_0 \xi_r^{t_i} \xi_r^{\Delta t} &= r_i \lambda_r, \\ z_{i+1} &= z_0 \xi_z^{t_i} \xi_z^{\Delta t} &= z_i \lambda_z. \end{aligned} \quad (2)$$

While the angle of rotation θ increases in arithmetic progression with the step $\Delta\theta$, the radius r forms a geometric progression with the scaling factor $\lambda_r = \xi_r^{\Delta t}$, and the vertical displacement z forms a geometric progression with the scaling factor $\lambda_z = \xi_z^{\Delta t}$. In many shells, parameters λ_r and λ_z are the same. Variations of shell shapes due primarily to different parameters of the helico-spiral are shown in Figure 2. They correspond closely to the shell types identified by d'Arcy Thompson [32, page 192].

2.2 The generating curve

The surface of the shell is determined by a generating curve C , sweeping along the helico-spiral \mathcal{H} . The size of the curve C increases as it revolves around the shell axis. The shape of C determines the profile of the whorls and of the shell opening. In order to capture the variety and complexity of possible shapes, we construct the generating curves from one or more segments of Bézier curves [9]. The impact of the generating curve on the shape of a shell is shown in Figures 3 and 4.

2.3 Incorporation of the generating curve into the model

The generating curve C is specified in a local coordinate system uvw . Given a point $\mathcal{H}(t)$ of the helico-spiral, C is first scaled up by the factor ξ_c^t with respect to the origin O of this system, then rotated and translated so that the point O matches $\mathcal{H}(t)$ (Figure 1). The axes uvw are used to orient the generating curve in space. The

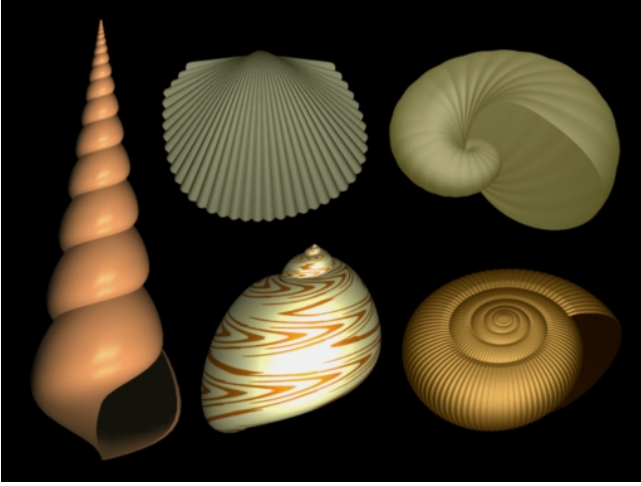


Figure 2: Variation of shell shapes resulting from different parameters of the helico-spiral. Leftmost: turbiniform shell ($z_0 = 1.9$, $\lambda = 1.007$). Top row: patelliform shell ($z_0 = 0$, $\lambda = 1.34$) and tubular shell ($z_0 = 0.0$, $\lambda = 1.011$). Bottom row: spherical shell ($z_0 = 1.5$, $\lambda = 1.03$) and diskoid shell ($z_0 = 1.4$, $\lambda = 1.014$). Values of $\lambda = \lambda_r = \lambda_z$ correspond to $\Delta\theta = 10^\circ$.

simplest approach is to rotate the system uvw so that the axes v and u become respectively parallel and perpendicular to the shell axis z . If the generating curve lies in the plane uv , the opening of the shell and the growth markings (such as the ribs on the shell surface) will be parallel to the shell axis. However, many shells exhibit approximately *orthoclinal* growth markings, which lie in planes normal to the helico-spiral \mathcal{H} [14]. This effect can be captured by orienting the axis w along the vector \vec{e}_1 , tangent to the helico-spiral at the point $\mathcal{H}(t)$. The curve is fixed in space by aligning the axis u with the principal normal vector \vec{e}_2 of \mathcal{H} . The unit vectors \vec{e}_1 and \vec{e}_2 can be calculated using the following formulae [3]:

$$\vec{e}_1 = \frac{\vec{\mathcal{H}}'(t)}{|\vec{\mathcal{H}}'(t)|}, \quad \vec{e}_3 = \frac{\vec{e}_1 \times \vec{\mathcal{H}}''(t)}{|\vec{e}_1 \times \vec{\mathcal{H}}''(t)|}, \quad \vec{e}_2 = \vec{e}_3 \times \vec{e}_1. \quad (3)$$

Symbols $\vec{\mathcal{H}}'(t)$ and $\vec{\mathcal{H}}''(t)$ denote the first and the second derivative of the position vector $\vec{\mathcal{H}}(t)$ of the point $\mathcal{H}(t)$, taken with respect to the parameter t . Vectors \vec{e}_1 , \vec{e}_2 and \vec{e}_3 define a local orthogonal coordinate system called the *Frenet frame*. It is considered a good reference system for specifying orientation, because it does not depend on the parametrization of the helico-spiral \mathcal{H} or on the coordinate system in which it is expressed [7]. The Frenet frame is not defined in the points with zero curvature, but a helico-spiral has no such points ($\mathcal{H}''(t)$ is never equal to zero). The impact of the orientation of the generating curve is illustrated in Figure 5. The opening of the real shell and the ribs on its surface lie in planes normal to the helico-spiral. This is properly captured in the model in the center, which uses Frenet frames to orient the generating curve. The model on the right incorrectly aligns the generating curve with the shell axis.

In general, the generating curve need not be aligned either with the shell axis or with the Frenet frame. In the case of non-planar generating curves, it is even difficult to define what the “alignment” could mean. It is therefore convenient to be able to adjust the orientation of the generating curve with respect to the reference coordinate system. We accomplish this by allowing the user to specify a rotation of the system uvw with respect to each of the axes \vec{e}_1 , \vec{e}_2 , and \vec{e}_3 .



Figure 3: Variation of the shell shape resulting from different generating curves. From left to right: turreted shell, two fusiform shells, and a conical shell.

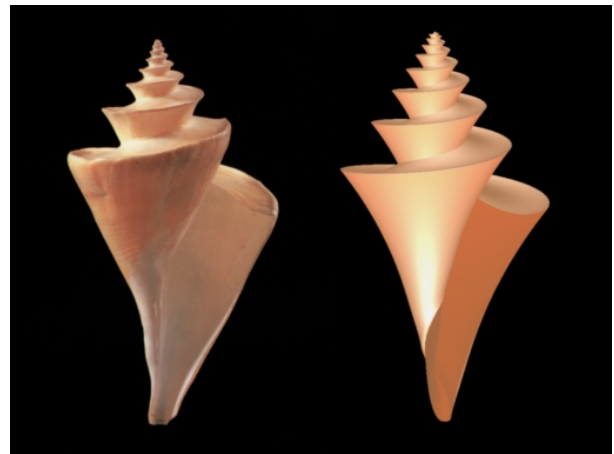


Figure 4: A photograph [12, page 97] and a model of *Thatcheria mirabilis* (Miraculous Thatcheria). The unusual shape of this shell results from the triangular generating curve. Photograph by courtesy of The Natural History Museum, London, England.



Figure 5: A photograph [12, page 47] and two models of *Epitonium scalare* (Precious Wentletrap). Photograph by courtesy of Ken Lucas, Biological Photo Service, Moss Beach, California.

2.4 Construction of the polygon mesh

In the mathematical sense, the surface of the shell is completely defined by the generating curve \mathcal{C} , sweeping along the helico-spiral \mathcal{H} . Nevertheless, we represent this surface as a polygon mesh for rendering purposes. The mesh is constructed by specifying $n+1$ points on the generating curve (including the endpoints), and connecting corresponding points for consecutive positions of the generating curve. The sequence of polygons spanned between a pair of adjacent generating curves is called a *rim*.

The reaction-diffusion equations describing pigmentation patterns, to be discussed in Section 3, can be solved the easiest way if the (one-dimensional) space in which they operate is discretized uniformly. This corresponds to the partition of the rim into polygons evenly spaced along the generating curve. A suitable partitioning method was described by Bartels and Hardtke [2] and is summarized below.

Let $\mathcal{C}(s) = (u(s), v(s), w(s))$ denote a parametric definition of the curve \mathcal{C} in coordinates uvw , with $s \in [s_{min}, s_{max}]$. The length of an arc of \mathcal{C} is related to an increment of parameter s by the equations:

$$\frac{dl}{ds} = f(s), \quad (4)$$

$$f(s) = \sqrt{\left(\frac{du}{ds}\right)^2 + \left(\frac{dv}{ds}\right)^2 + \left(\frac{dw}{ds}\right)^2}. \quad (5)$$

The total length L of \mathcal{C} can be found by integrating $f(s)$ in the interval $[s_{min}, s_{max}]$:

$$L = \int_{s_{min}}^{s_{max}} f(s) ds. \quad (6)$$

Inversion of the equation (4) yields:

$$\frac{ds}{dl} = \frac{1}{f(s)}. \quad (7)$$

Given the initial condition $s(0) = s_{min}$, this first-order differential equation describes parameter s as a function of the arc length l . By numerically integrating (7) in n consecutive intervals of length $\Delta l = \frac{L}{n}$, we obtain a sequence of parameter values $s_0 = s_{min}, s_1, s_2, \dots, s_n = s_{max}$, representing the desired sequence of $n+1$ polygon vertices equally spaced along the curve \mathcal{C} . The effect of the reparametrization of the generating curve is shown in Figure 6.

The same figure reveals unequal spacing of polygon vertices between adjacent generating curves. The polygons are stretched horizontally in the wide central portions of the shells, and squeezed near the top and the bottom. This effect is due to the differences in the lengths of the trajectories traced by different points on the generating curve in equal time intervals. A reparametrization of trajectories by their arc length would yield a uniform distribution of vertices along each trajectory, but the benefits of such operation are not certain. Specifically, it is not clear whether the progress of the reaction-diffusion process along a trajectory depends directly on its length, the progress of time, or a combination of both factors. In the context of *Nautilus pompilus* this problem has been discussed by Meinhardt and Klinger [18].

2.5 Modeling the sculpture on shell surfaces

Many shells have a sculptured surface. Common forms of sculpturing include ribs parallel to the direction of growth or to the generating curve. Both types of ribs can be easily reproduced by

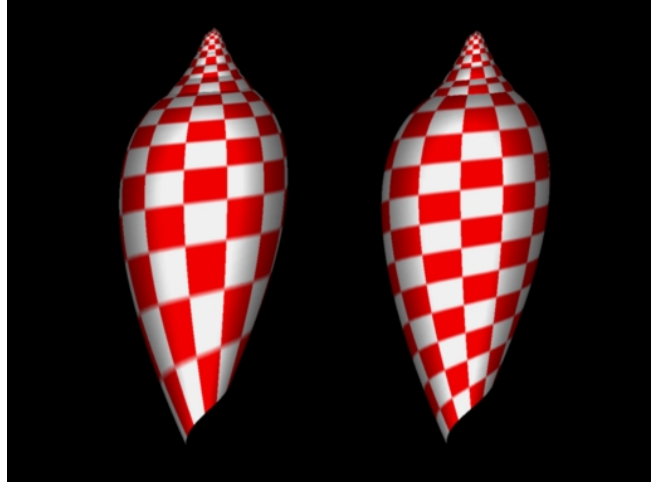


Figure 6: The effect of the reparametrization of the generating curve. In the left shell, mesh vertices are spaced along the generating curve using constant increments of the parameter s . In the right shell, the increments of parameter s have been adjusted to divide the generating curve into segments of equal length. As a result, texture distortion along the generating curve has been eliminated.

displacing the vertices of the polygon mesh in the direction normal to the shell surface.

In the case of ribs parallel to the direction of growth, the displacement d varies periodically along the generating curve. The amplitude of these variations is proportional to the actual size of the curve, thus it increases as the shell grows. Sample applications of this technique are depicted in Figures 7, 8, and 9.

The periodic displacement along the generating curve could be incorporated into the curve definition, but we chose to capture the displacement independently from the overall shape of \mathcal{C} . This approach is more flexible and can be easily extended to other sculptured patterns. For example, oblique ribs oriented diagonally with respect to the generative curve (as in *Strigilla carnea* [18]) result from a gradual incrementation of the phase of the periodic displacement during the shell's growth.

Ribs parallel to the generating curve are obtained by periodically varying the value of the displacement d according to the position of the generating curve along the helico-spiral \mathcal{H} . As previously, the amplitude is proportional to the current size of the generating curve. Examples are shown in Figure 10. The two shells on the right side have ribs parallel to the generating curve. The shells on the left display latticed sculpturing, obtained by superimposing ribs parallel to the generating curve and to the direction of growth.

3 GENERATION OF PIGMENTATION PATTERNS

Pigmentation patterns constitute an important aspect of shell appearance. We propose to capture them using a class of reaction-diffusion models developed by Meinhardt and Klinger [17, 18, 19, 20]. A summary of this approach is presented below in order to make our description of shell modeling complete.

Pigmentation patterns in shells show enormous diversity. From the perspective of mollusc evolution, this diversity is attributed to the lack of selective value of any particular pattern. In many cases, the animals live burrowed in sand, or are active at night. Sometimes the pattern is invisible as long as the animal is alive, due to a covering



Figure 7: A photograph [30, entry 326] and a model of *Rapa rapa* (Papery Rapa) showing surface sculpturing with the ribs orthogonal to the generating curves. The shape of ribs in the model is captured by a sine function uniformly spaced along the edge of the shell.

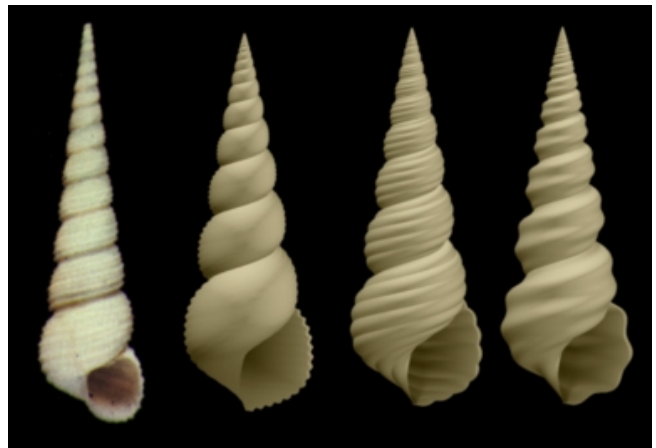


Figure 9: Surface sculpturing with the ribs orthogonal to the generating curves. A photograph [30, entry 128] and three models of *Turritella nivea* illustrate the effect of the decreasing frequency of the modulating function.



Figure 8: A photograph [30, entry 22] and a model of *Cardium costatum* (Ribbed Cockle)

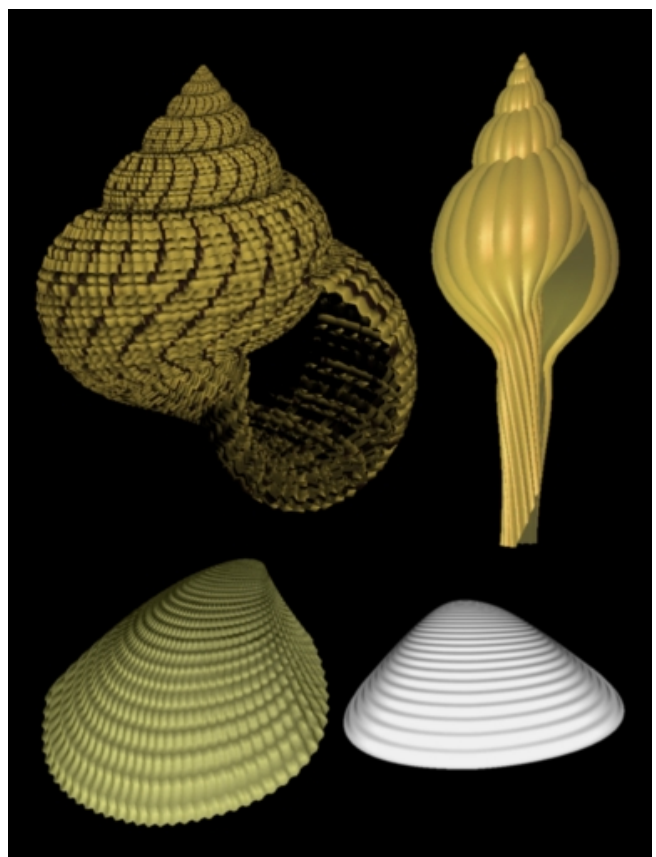


Figure 10: Surface sculpturing with the ribs parallel to the generating curve (right) and with a lattice of ribs (left)

by non-transparent layers. Consequently, there is no evolutionary pressure giving a preference to specific patterns.

The diversity of the patterns, which may differ in details even between shells of the same species, suggests a morphogenetic mechanism general enough to encompass large specimen-to-specimen and species-to-species variations. We assume that it is of the reaction-diffusion type [11, 16, 33]. Pigment deposition is under the control of a substance, called the *activator*, which stimulates its own production through a positive feedback mechanism, or *autocatalysis*. In order for a pattern to be formed, a mechanism is also needed for suppressing the production of the activator in the neighborhood of the autocatalytic centers. This prevents the activator from spreading over the entire substrate. Thus, the pattern is formed as a result of the antagonistic interaction between short-range activation and long-range inhibition.

Harrison [13] points out that reaction-diffusion is not a single model, but the cornerstone of a whole spectrum of models, differing in the number and characteristics of the reacting substances. This observation remains true for the models of pigmentation patterns in shells. We do not capture all possible patterns in a single system of equations, but modify it according to the specific pattern. Generally, we group our models into two basic categories distinguished by Gierer and Meinhardt [11]: activator-substrate, and activator-inhibitor.

3.1 The activator-substrate model

The inhibitory effect may result from the depletion of the substrate required to produce the activator. A possible interaction is described by the following equations:

$$\begin{aligned} \frac{\partial a}{\partial t} &= \rho s \left(\frac{a^2}{1 + \kappa a^2} + \rho_0 \right) - \mu a + D_a \frac{\partial^2 a}{\partial x^2} \\ \frac{\partial s}{\partial t} &= \sigma - \rho s \left(\frac{a^2}{1 + \kappa a^2} + \rho_0 \right) - \nu s + D_s \frac{\partial^2 s}{\partial x^2} \end{aligned} \quad (8)$$

The activator, with the concentration a , diffuses along the x -axis at the rate D_a and decays at the rate μ . Similarly, the substrate, with the concentration s , diffuses at the rate D_s and decays at the rate ν . The substrate is produced at a constant rate σ . Production of the activator is an autocatalytic process, proportional to a^2 for small activator concentrations. This process can take place only in the presence of the substrate, and decreases its amount. Parameter ρ is the coefficient of proportionality. The autocatalysis can saturate at high activator concentrations, at the level controlled by the parameter κ . Parameter ρ_0 represents a small base production of the activator, needed to initiate the autocatalytic process.

Figure 11 shows the application of equations (8) to the formation of stripes parallel to the direction of shell growth. In order to start the pattern formation process, parameter ρ is subject to small random fluctuations (less than 2.5% of its average value) for the individual cells. The pattern that emerges after the initial transition is stable in time, but periodic in space. This periodicity is achieved by setting the range of inhibition (determined by the diffusion and decay rates of the substrate) to a fraction of the total length of the growing edge.

In order to solve the equations and generate the images, the growing edge is divided into cells of length Δx . In the planar representation of the pattern on the left side of Figure 11, the cells correspond to a horizontal row of pixels. In the shell on the right the cells correspond to the polygons on the growing edge. The equations are solved using the forward Euler method [10] (a FORTRAN code is included in the paper [19]). We ignore the effect of the gradual increase of polygon size resulting from the rim's growth.

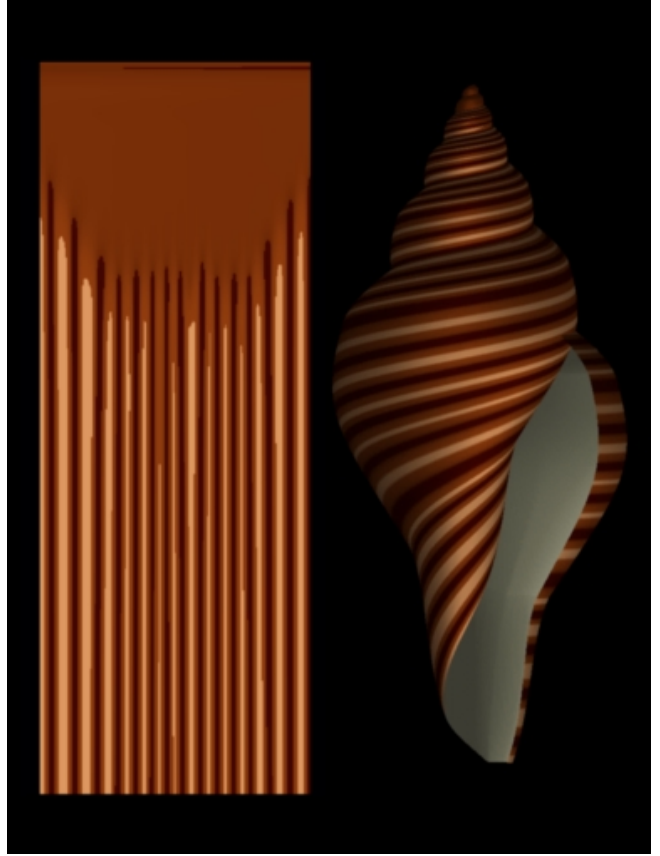


Figure 11: A stable pattern of stripes generated by the activator-substrate model using equations (8), with $\rho = 0.01 \pm 2.5\%$, $\rho_0 = 0.001$, $\mu = 0.01$, $D_a = 0.002$, $\sigma = 0.015$, $\nu = 0$, $D_s = 0.4$, and $\kappa = 0$

Concentrations of the activator corresponding to fixed time intervals Δt determine colors of cells in the consecutive rows or rims.

The generation of stripes using the activator-substrate model is interesting from the theoretical perspective, since it illustrates the emergence of a pattern from an almost uniform initial distribution of substances (the solid area in the upper part of the planar representation in Figure 11). The development of a pattern in a homogeneous medium motivated the original definitions and studies of the reaction-diffusion models [11, 33]. In order to demonstrate their practical usefulness for the synthesis of shell images, we must consider more complex patterns than stripes.

Figure 12 shows a photograph and a model of *Amoria undulata*. The pattern consists of wavy lines that, on the average, run in the direction parallel to the growing edge. This direction is partially obscured by the large amplitude of the waves. The periodic character of the pattern in the direction of the helico-spiral is a manifestation of the oscillations of the activator concentration over time. In the activator-substrate model they are known to occur for $\sigma < \mu$ [17]. In order to generate lines of undulating shape, we assume that the activator-substrate process is regulated by an external factor, which modulates the substrate production σ according to a periodic (sine) function of cell position, $\sigma = \sigma(x)$. Undulations occur, since in regions with higher σ oscillations are faster than in regions with lower σ values. The coherence of the lines is maintained by the diffusion of the activator. Higher diffusion constants force better synchronization between the neighboring cells, yielding lines that follow the orientation of the growing edge more closely.



Figure 12: A photograph [30, entry 222] and a model of *Amoria undulata* (Waved Volute). Generated using equations (8), with $\rho = 0.1 \pm 2.5\%$, $\rho_0 = 0.005$, $\mu = 0.1$, $D_a = 0.004$, $\sigma_{max} = 0.012$, $\nu = 0$, $D_s = 0.0$, and $\kappa = 1$.



Figure 13: A photograph [30, entry 132] and a model of *Volutoconus bednalli* (Bednall's Volute). Generated using equations (8), with $\rho = 0.1 \pm 2.5\%$, $\rho_0 = 0.0025$, $\mu = 0.1$, $D_a = 0.01$, $\sigma_{max} = 0.11$, $\nu = 0.002$, $D_s = 0.05$, and $\kappa = 0.5$.

Volutoconus bednalli, shown in Figure 13, displays a variant of the same mechanism. In this case, the function $\sigma(x)$ periodically exceeds the decay constant of the activator, producing stripes of cells with permanently high activator concentration. The oscillating patterns between these stripes can be viewed as traveling waves that annihilate each other as they meet.

3.2 The activator-inhibitor model

Propagation of colliding waves is the essential feature of the pigmentation pattern of *Oliva porphyria*, presented in Figure 14. The oblique lines represent waves of activator concentration, traveling along the growing edge. As previously, colliding waves extinguish each other. In Figure 14, this corresponds to an element of the pattern in the shape of the symbol <. Another element of this pattern is a branch that occurs when an activated point of one wave spontaneously initiates another wave, traveling in the opposite direction.

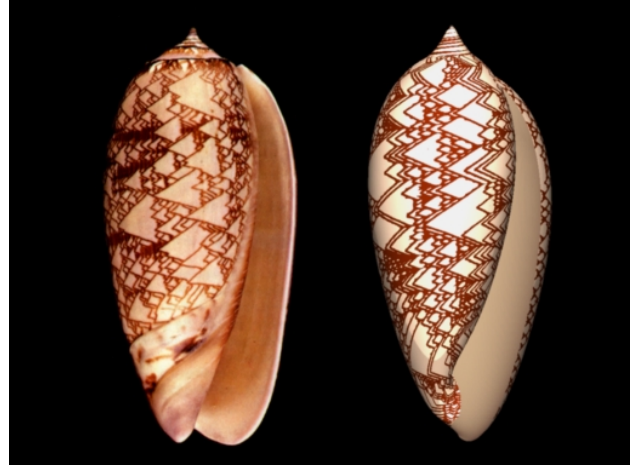


Figure 14: A photograph [30, entry 83] and a model of *Oliva porphyria*. Generated using equations (9), with $\rho = 0.1 \pm 2.5\%$, $\rho_0 = 0.0001$, $\mu = 0.1$, $D_a = 0.015$, $\sigma = 0.0002$, $\nu = 0.014$, $D_h = 0.0$, $\rho' = 0.1$, $\eta = 0.1$, $h_0 = 0.1$, and $\kappa = 0.25$.



Figure 15: A photograph [30, entry 240] and a model of *Conus marmoreus* (Marble Cone)

Observation of the shell indicates that the number of traveling waves is approximately constant over time. This suggests a global control mechanism that monitors the total amount of activator in the system, and initiates new waves when its concentration becomes too low. This mechanism can be captured using the following system of equations:

$$\begin{aligned}\frac{\partial a}{\partial t} &= \frac{\rho}{h + h_0} \left(\frac{a^2}{1 + \kappa a^2} + \rho_0 \right) - \mu a + D_a \frac{\partial^2 a}{\partial x^2} \\ \frac{\partial h}{\partial t} &= \sigma + \rho \frac{a^2}{1 + \kappa a^2} - \frac{\nu}{c} h + D_h \frac{\partial^2 h}{\partial x^2} \\ \frac{dc}{dt} &= \frac{\rho'}{x_{max} - x_{min}} \int_{x_{min}}^{x_{max}} a dx - \eta c\end{aligned}\quad (9)$$

The first two equations represent an activator-inhibitor system. As with the activator-substrate model, production of the activator is an autocatalytic process. The activator also catalyzes the production of

its antagonist, the inhibitor h , which in turn decreases the production of the activator proportionally to $1/(h+h_0)$. We postulate that this process is globally regulated by a hormone c , which monitors the total amount of activator along the growing edge. The hormone diffuses much faster than the remaining substances, thus its concentration along the growing edge is assumed to be constant. A small number of traveling waves yields a small concentration of the hormone, which accelerates the decay of the inhibitor h . The concentration of the activator increases and at some points reaches the threshold at which new waves are formed. This is a self-regulating process, where the hormone c provides a negative feedback maintaining the number of traveling waves at an approximately constant level.

The model of *Conus marmoreus*, shown in Figure 15, is similar to that of *Oliva*. The pigment producing process is controlled by another reaction-diffusion process, instead of a hormone. Models of several other patterns are presented in detail by Meinhardt and Klinger [18, 19].

4 CONCLUSIONS

This paper presents a comprehensive model of seashells, suitable for computer imagery purposes. The model combines separate results described in the existing paleontological, biological, and computer graphics literature into a single model, capable of generating relatively realistic images of many shells. The overall shape of a shell is determined by the parameters of the helico-spiral and the generating curve. The sculpturing is obtained by periodically displacing vertices of the polygon mesh representing the shell surface. Attention is given to details, such as the orientation of the axial ribs and the shell opening, and prevention of distortions of the sculptured and pigmented patterns. Pigmentation is simulated using reaction-diffusion models. A comparison of the results with the photographs of real shells shows good correspondence of the shapes and the patterns. This is important both from the visual perspective and from the viewpoint of the applications of the models to biology. Direct observation of phenomena such as the postulated flow of a hormone in *Oliva* is difficult, and agreement of synthetic images with reality indirectly supports the models. Realistic visualization makes such comparisons more convincing.

Comparisons with the real shells also reveal shortcomings of our models, leading to problems open for further research:

- *Proper modeling of the shell opening.* The sweeping of a uniformly growing generating curve along the helico-spiral produces a strictly self-similar surface that can be mapped into itself by a scaling and a rotation around the shell axis [6, 31]. In real shells, the lips at the shell opening often display a departure from self-similarity. *Strombus listeri*, on the left side of Figure 16, provides a striking example of this phenomenon, although to a lesser extent it also occurs in other shells, such as *Volutococonus bednalli* and *Oliva porphyria* (Figures 13 and 14). The modeling of the shell opening requires further investigation.
- *Modeling of spikes.* The model of shell sculpture, based on the perturbation of the surface in the direction of the normal vector, is an appropriate technique for reproducing relatively small ridges. It does not capture large modifications of the shape, such as spikes in *Murex pecten* and extrusions in *Chicoreus spectrum* (Figure 16). The incorporation of these structures into the models remains an open problem.
- *Capturing the thickness of shell walls.* We represent a shell wall as a single surface, albeit its two sides are rendered differently. In reality, the wall has some thickness, which

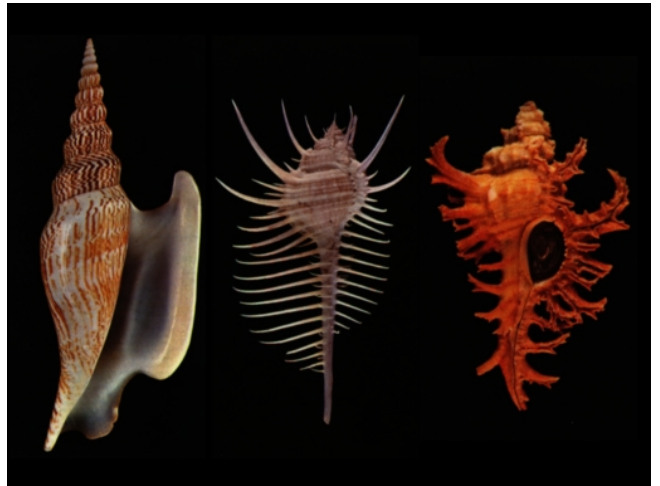


Figure 16: Photographs [30, entries 113, 276 and 29] of three shells that exemplify the main limitations of the present model. From left to right: *Strombus listeri* (Lister's Conch), *Murex pecten* (Venus Comb Murex), and *Chicoreus spectrum* (Ghost Murex).

should be reproduced to properly visualize the edge of the shell opening.

- *Alternatives to the integrated model.* The integration of pigmentation patterns into the shell model is an appealing feature from the biological perspective, since it is consistent with the developmental nature of the models. Unfortunately, it also leads to large polygon meshes, necessary to capture the intricacies of the patterns. In our implementation, the meshes may consist of millions of polygons. This creates rendering problems, because the renderer may impose limits on the maximum size of the mesh. Separate generation of the shell shape and the pigmentation pattern, combined into a single image using texture mapping, may represent a preferable approach.
- *Improved rendering.* A comparison of the photographs of real shells with the synthetic images of their models exhibits the need for a better rendering technique. Specifically, it could capture the anisotropic highlights, the translucency of shell walls, and the darkening inside the shell opening.

Solutions to all of these problems seem to be achievable. They should improve our understanding of the forms and patterns of shells, and bring us closer to photorealism.

Acknowledgements

This research was sponsored by an operating grant from the Natural Sciences and Engineering Research Council of Canada, and by a graduate scholarship from the University of Regina. We are indebted to Pat Hanrahan for providing Deborah with the access to his research facilities at Princeton, and to Jim Hanan for recording the images at the University of Regina. Photographs of real shells included in Figures 7, 8, 9, 12, 13, 14, 15, and 16 are reproduced with the kind permission of Giuseppe Mazza. We would like to thank the anonymous referees for many useful comments on the first version of this paper.

References

- [1] R. Baker and G. T. Herman. Simulation of organisms using a developmental model, parts I and II. *Int. J. of Bio-Medical Computing*, 3:201–215 and 251–267, 1972.
- [2] R. Bartels and I. Hardtke. Speed adjustment for key-frame interpolation. In *Proceedings of Graphics Interface '89*, pages 14–19, 1989.
- [3] W. Bronsvoort and F. Klok. Ray tracing generalized cylinders. *ACM Transactions on Graphics*, 4(4):291–303, 1985.
- [4] T. A. Cook. *Curves of Life*. Dover Publications, New York, 1979. Originally published in 1914, by Constable and Company, London.
- [5] M. B. Cortie. Models for mollusc shell shape. *South African Journal of Science*, 85:454–460, 1989.
- [6] H. S. M. Coxeter. *Introduction to Geometry*. J. Wiley & Sons, New York, 1961.
- [7] M. do Carmo. *Differential Geometry of Curves and Surfaces*. Prentice Hall, Englewood Cliffs, 1976.
- [8] B. Ermentrout, J. Campbell, and G. Oster. A model for shell patterns based on neural activity. *The Veliger*, 28:369–388, 1986.
- [9] J. D. Foley, A. van Dam, S. Feiner, and J. Hughes. *Computer graphics: Principles and practice*. Addison-Wesley, Reading, 1990.
- [10] L. Fox and D. F. Mayers. *Numerical Solution of Ordinary Differential Equations*. Chapman and Hall, London, 1987.
- [11] A. Gierer and H. Meinhardt. A theory of biological pattern formation. *Kybernetik*, 12:30–39, 1972.
- [12] N. R. Gordon. *Seashells: A Photographic Celebration*. Friedman Group, New York, 1990.
- [13] L. G. Harrison. What is the status of the reaction-diffusion theory thirty-four years after Turing? *Journal of Theoretical Biology*, 125:369–384, 1987.
- [14] C. Illert. Formulation and solution of the classical seashell problem. *Il Nuovo Cimento*, 11 D(5):761–780, 1989.
- [15] Y. Kawaguchi. A morphological study of the form of nature. *Computer Graphics*, 16(3):223–232, 1982.
- [16] H. Meinhardt. *Models of Biological Pattern Formation*. Academic Press, London, 1982.
- [17] H. Meinhardt. Models for positional signalling, the threefold subdivision of segments and the pigmentation pattern of molluscs. *Journal of Embryology and Experimental Morphology*, 83:289–311, 1984.
- [18] H. Meinhardt and M. Klinger. A model for pattern formation on the shells of molluscs. *Journal of Theoretical Biology*, 126:63–89, 1987.
- [19] H. Meinhardt and M. Klinger. Pattern formation by coupled oscillations: The pigmentation patterns on the shells of molluscs. In *Lecture Notes in Biomathematics*, volume 71, pages 184–198. Springer-Verlag, Berlin, 1987.
- [20] H. Meinhardt and M. Klinger. Schnecken- und Muschelschalen: Modellfall der Musterbildung. *Spektrum der Wissenschaft*, pages 60–69, August 1991.
- [21] H. Moseley. On the geometrical forms of turbinated and discoid shells. *Philosophical Transactions of the Royal Society of London*, pages 351–370, 1838.
- [22] J. D. Murray. *Mathematical Biology*. Springer-Verlag, Berlin, 1989.
- [23] P. Oppenheimer. Real time design and animation of fractal plants and trees. *Computer Graphics*, 20(4):55–64, 1986.
- [24] C. A. Pickover. A short recipe for seashell synthesis. *IEEE Computer Graphics and Applications*, 9(6):8–11, 1989.
- [25] C. A. Pickover. *Computers and the Imagination*. St. Martin's Press, New York, 1991.
- [26] P. Prusinkiewicz and D. Streibel. Constraint-based modeling of three-dimensional shapes. In *Proceedings of Graphics Interface '86 — Vision Interface '86*, pages 158–163, 1986.
- [27] D. M. Raup. Computer as aid in describing form in gastropod shells. *Science*, 138:150–152, 1962.
- [28] D. M. Raup. Modeling and simulation of morphology by computer. In *Proceedings of the North American Paleontology Convention*, pages 71–83, 1969.
- [29] D. M. Raup and A. Michelson. Theoretical morphology of the coiled shell. *Science*, 147:1294–1295, 1965.
- [30] B. Sabelli. *Guide to Shells*. Simon & Schuster, New York, 1979. Edited by H. S. Feinberg.
- [31] d'Arcy Thompson. *On Growth and Form*. University Press, Cambridge, 1952.
- [32] d'Arcy Thompson. *On Growth and Form, Abridged Edition*. University Press, Cambridge, 1961.
- [33] A. Turing. The chemical basis of morphogenesis. *Philosophical Transactions of the Royal Society of London B*, 237:37–72, 1952.
- [34] G. Turk. Generating textures on arbitrary surfaces using reaction-diffusion. *Computer Graphics*, 25(4):289–298, 1991.
- [35] C. H. Waddington and J. Cowe. Computer simulations of a molluscan pigmentation pattern. *Journal of Theoretical Biology*, 25:219–225, 1969.
- [36] A. Witkin and M. Kass. Reaction-diffusion textures. *Computer Graphics*, 25(4):299–308, 1991.
- [37] S. Wolfram. Cellular automata as models for complexity. *Nature*, 311:419, 1984.